Determining the Air Void Parameters of Concrete Using Digital Image Analysis of Polarized Light Micrographs

Michael Scott

Thesis submitted to the Faculty of the

Virginia Polytechnic Institute and State University

in partial fulfillment of the requirements for the degree of

Master of Science

in

Engineering Mechanics

Dr. John C. Duke, Jr.
Dr. Richard Weyers
Dr. Edmund G. Henneke

April 22, 1997

Blacksburg, Virginia

Keywords:

Concrete, image analysis, powers spacing factor, microscopy.

Copyright

Abstract

The ASTM C457 test has long been a standard used to obtain the air void parameters of concrete materials. These air void parameters provide valuable information that has been linked to the performance of concrete under conditions such as freezing and thawing cycles. The standard test procedure involves linearly traversing a cut and polished section of a concrete specimen while a technician observes it under a microscope. Chord lengths of material constituents that the technician observes along the linear traverse are recorded and later used to calculate air void parameters statistically. This procedure is long and tedious, which makes it susceptible to human error due to operator fatigue.

This study proposes and implements a new test method for evaluating concrete air void parameters using an image analysis method. A polishing procedure along with a differential interference contrast microscope are used to obtain high contrast images of material constituents, which provide raw data for the image analysis method. Because of the high contrast that can be obtained, cement paste, air voids in the cement paste, and aggregate materials in the concrete can be distinguished from one another based on these images. An image analysis program has been written for this study which linearly traverses these images and records the chord lengths of material constituents in a similar way to the standard ASTM C457 test. The chord length data must be processed further, however, because features in the images can be truncated by the edge of the image. Correction calculations for this problem are implemented in the image analysis algorithm.

Two specimens which have been previously tested using the standard ASTM C457 method by the Virginia Transportation Research Council, (VTRC), are used in this study. The air void parameters obtained using the new test are compared directly with the results obtained by VTRC for the two specimens. Statistical comparisons indicate that the results of the new test are indeed significant, showing the potential it has for practical implementation. There are drawbacks to the test including a long polishing procedure, but this process can be automated. The new test appears to have excellent potential for practical application, but it should be emphasized that the test has only been implemented using materials in two concrete specimens. Further study on a variety of other concrete materials would be required for implementation in a standard procedure.

Acknowledgment

This report is a thesis presented by Michael L. Scott in partial fulfillment of the requirements for the Master of Science degree. Support for this research was provided by the National Science Foundation Center for Infrastructure Assessment and Evaluation at Virginia Tech.

The experiences I have had in the course of attending graduate school have taken me to places I never would have expected. I have been fortunate to have Dr. Duke as my advisor along the way. He has shown me a great deal as a teacher and as an example of a true professional. I am also grateful to Dr. Weyers for his good advice, "war stories", and technical help. Others I would like to thank for help on this project include Steve Lane (Virginia Transportation Research Council), Dr. Abbott (EE Department), Farooq Azam (EE Department), Jerzy Zemajtis and Wioleta Pyc (Civil Department), and Dr. Craig (Geology Department). I would also like to thank Marc Schultz for being a true friend. Finally, I am grateful to my parents, Marion and Linda Scott, and my brother, Stephen Scott, for their constant support.

Table of Contents

Page

List of Figures

Chapter 1 - Introduction

1.1 - Scope

This study has resulted from a desire to evaluate concrete air void parameters quickly and accurately. The current standard method for making these evaluations, the ASTM C457 test, is time consuming and requires the judgement of an expert technician. A variety of methods have been proposed and studied to overcome the problems inherent in the standard test, but none has been shown to be practical for effectively replacing the current ASTM C457 procedure. Before undertaking this work, many of the methods which had been studied previously were examined on a trial basis to assure that an effective procedure had not already been implemented.

One of these methods involved impregnating concrete materials with a polymeric material that contained flourescent particles. This allowed researchers to easily locate air void spaces in concrete when an ultraviolet light source was incident on a specimen, providing excellent information. Unfortunately, this method did not allow aggregate materials to be distinguished from cement paste materials in the concrete. Without this capability, a practical determination of concrete air void parameters is not possible unless an expert technician is used. Other methods such as acoustic microscopy, profilometry, and infrared imaging were explored in an attempt to distinguish the material constituents in concrete. These methods offered some possibilities, but none of them consistently displayed contrast between the cement paste, aggregate, and void constituents of concrete.

The differential interference contrast microscopy technique that was eventually implemented in this study did display excellent contrast between concrete constituents. This cabability indicated that an image analysis procedure for determining air void parameters was indeed possible. The motivation for determining concrete air void parameters using this technique is provided in the following sections.

1.1.1 - Concrete and freeze-thaw durability

Concrete materials are frequently used in applications where freezing and thawing cycles occur. During these cycles the concrete can expand and contract significantly, which is caused by water in the microstructure changing between solid and liquid states. These expansions and contractions of the material can fatigue the concrete microstructure over time and may lead to the disintegration and failure of the material. The internal pressures that are generated in the concrete as the water changes state can, however, be relieved. This is usually accomplished by creating air voids in the cement paste using air entraining admixtures.

Concrete applications where freezing and thawing cycles often occur include bridge decks and structural members, highway pavements, sidewalks, and many other infrastructure components. When these concrete components are exposed to very frequent cycles of freezing and thawing, problems with durability may become quite pronounced. The distribution and size of entrained air voids in the concrete is critical to preserving the integrity of the cement paste microstructure under these conditions. Descriptions of the basic constituents of concrete in the following sections will clarify the physical mechanisms that contribute to the freeze-thaw degradation process.

1.2.1 - Hardened concrete structure

The material structure of hardened concrete consists of four basic constituents which must be distinguished from one another in order to understand concrete's freeze-thaw behavior. As shown in Figure 1 these four constituents are the hardened cement paste, aggregate, entrained air voids, and entrapped air voids (ASTM ‘93). Hardened cement paste is the binding material in concrete, and consists of several crystalline calcium compounds and associated water which is bound to these crystals through ionic bonding and van der waals forces. The bulk of the calcium compounds in the paste make up a calcium silicate hydrate gel, but calcium hydroxide and other calcium compounds are also present. Depending on the formulation of the concrete, a significant portion of the water in the

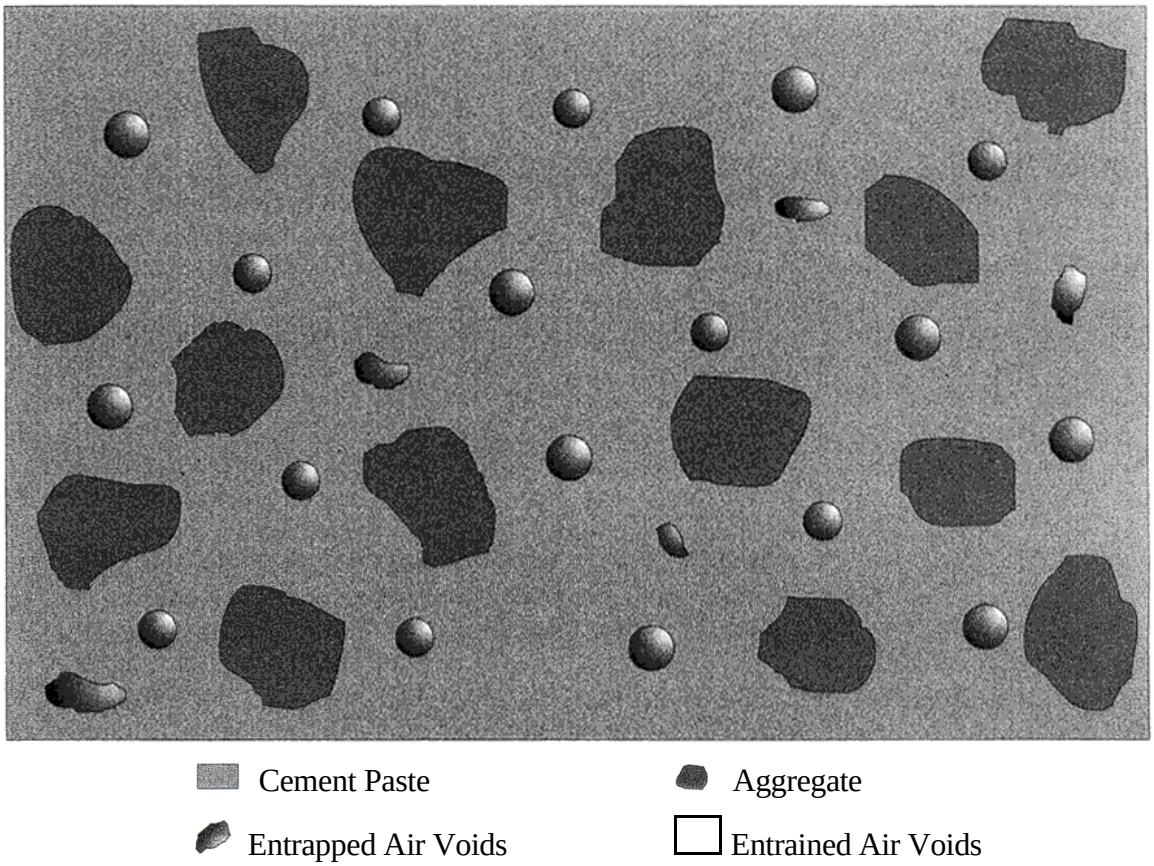

Figure 1. A simplified drawing of the four basic constituents of concrete viewed in a cross section through the material.

cement paste can be very loosely bound and may be termed free water. This free water will have a significant effect on the freeze-thaw behavior of concrete.

The aggregate constituent of concrete consists of granular materials such as sand, gravel or crushed stone. These aggregates are almost always made up of natural minerals which have been processed and sorted based on their physical, chemical and geometric properties. Mehta notes that carbonate rocks comprise about two-thirds of crushed aggregate used in the United States, while sandstone, granite, diorite, gabbro, and basalt make up the rest. He goes on to mention that natural silica sand is usually used for fine aggregate, which is used when very small aggregate sizes are desirable.

Air voids in concrete are cavities in the hardened cement paste that are produced by either the physical mixing process or air entraining admixtures. When these voids are produced by the physical mixing process they are termed entrapped, while voids created by chemical admixtures are termed entrained. Entrapped air voids can typically be distinguished from entrained air voids based on both shape and size. Entrained air voids tend to be spherical in shape, while entrapped air voids have very irregular shapes.

Entrapped air voids also tend to be larger than one millimeter, while entrained air voids are almost always smaller than one millimeter.

1.2.2 - Air voids and freeze-thaw resistance

Work by Powers, Philleo and a number of other scientists have led to the general consensus that properly entrained air voids can produce concrete with a highly improved freeze-thaw durability (Mehta). This improvement in durability is better understood when the generally accepted freeze-thaw degradation theory has been reviewed. Powers stated that the degradation is caused by a combination of hydraulic and osmotic pressures. These pressures are induced by the increase in volume that water experiences when it changes from a liquid phase to a solid phase. Figure 2 shows typical results of hydraulic and osmotic pressures when they are repeatedly induced in cement paste.

As Figure 2 illustrates, hydraulic pressures build up in the cement paste behind the freezing front when the water in the paste freezes and expands. The freezing front is the boundary between paste that contains frozen water and paste that still contains liquid water. According to Powers the magnitudes of hydraulic pressures depend on the distance to an "escape boundary", the permeability of the cement paste and the rate at which freezing takes place. Closely spaced entrained air voids have been shown to provide the "escape boundaries" Powers refers to. Osmotic pressures are also caused by freezing water in the paste, but in this case it is water in front of the freezing front that is increasing in pressure. The pressure increase is caused by partially frozen water expanding in cement paste capillary spaces. This freezing does not always take place at the same temperature, since ions in solution in the water can vary the freezing point of the capillary water. The pressures caused by both hydraulic and osmotic mechanisms will eventually lead to cracking in the cement paste if it freezes and thaws repeatedly without proper air entraining protection.

When pressure increases due to the hydraulic and/or osmotic phenomenon, it is due to a decrease in the volume available for the water to occupy in the concrete (Gutmann). In the absence of air voids, there is no local region of low pressure where the water in the cement paste can move. Pressure builds up as the water in the cement paste freezes, and a pressure gradient is observed beyond the freezing front. In this region beyond the freezing front, pressure is highest near the front and diminishes as water moves farther from the front. Air voids entrained in the cement paste provide a local means of relieving the pressures induced by both the hydraulic and osmotic mechanisms. If an air void is close

enough to the water in a region of the cement paste, the water can seep from the cement paste into the air void where the pressure is lower.

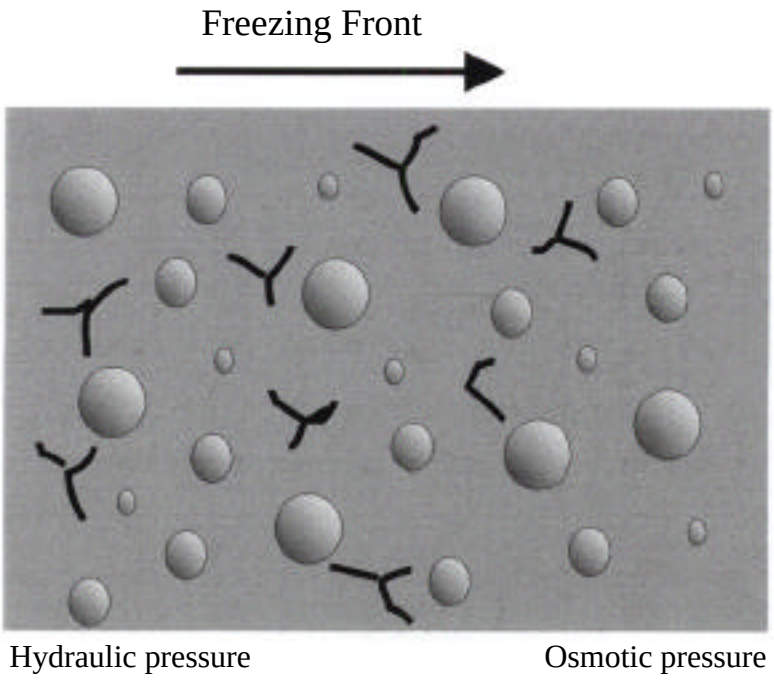

Figure 2. Cracking as a result of freeze-thaw cycles.

The function of entrained air voids, as previously described, is to provide pressure relief for water in the cement paste as it freezes. This pressure relief is only available to water in the paste that is located within a given proximity to the nearest air void. An area called the "protected paste" region describes the portion of the cement paste that is close enough to an air void that it can provide pressure relief for the water in that paste. This concept is clarified in Figure 3, where the protected paste regions are the light gray areas bounded by circular dashed lines. As in previous figures, cement paste is denoted by a dark gray region and entrained air voids are represented by circular areas with varying gray tone. This figure shows that the protected paste region lies at a fixed radial distance from the boundary of a particular entrained air void. If these protected regions overlap such that the entire paste region is covered, freeze-thaw durability is dramatically increased relative to an unprotected cement paste (Powers).

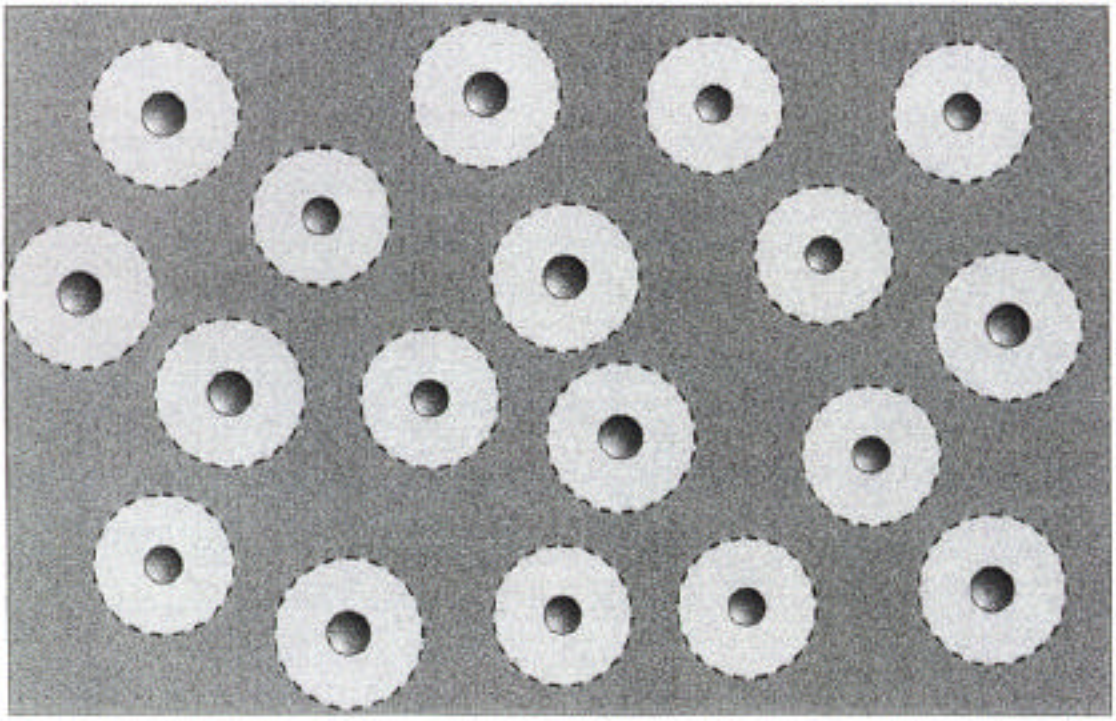

Figure 3. Illustration of the protected paste region.

Entrained air voids clearly play an important role in protecting concrete from freeze-thaw damage, but this information is of little use if the air void system cannot be controlled during batching and mixing. Fortunately, the types and amounts of air entraining admixtures can be selected to obtain repeatable air void systems in the cement paste. Many experimental studies have been conducted by Powers, Pigeon and others to establish clear links between these air void systems and measurable geometric parameters that reflect freeze-thaw durability. Two of these parameters, the Powers spacing factor and the Philleo factor, have become widely accepted as excellent predictors of freeze-thaw durability and are discussed in detail in the next section.

1.2.3 - Spacing factors

The Powers spacing factor and the Philleo factor were both developed by interpreting arrangements of loosely packed spheres. In the case of the Powers spacing factor, it is assumed that the spheres all have the same radius, (the mean radius), and are uniformly distributed in space. For visualization purposes, the simple cubic lattice model for a pure crystalline material has an identical geometry. In the context of this geometry, the

Powers spacing factor is half of the maximum distance between the boundaries of adjacent spheres, (S/2 as depicted in Figure 4). The Powers spacing factor provides an

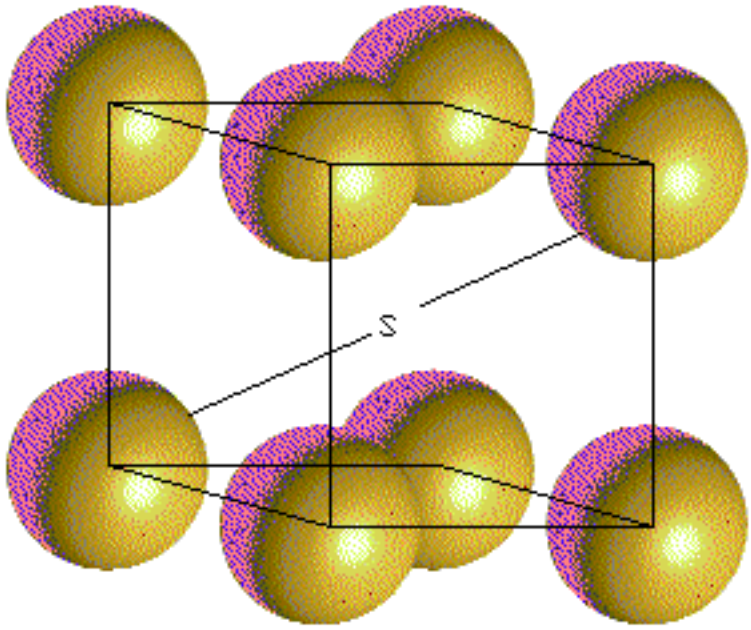

Figure 4. Graphical depiction of the Powers spacing factor, S/2.

approximate representation of the air void structure in the cement paste. The physical reality is that the entrained air voids are randomly distributed in the cement paste. This is an important difference, but the approximations inherent in the Powers spacing factor have been shown to be quite good in most cases. Situations where Powers spacing factor can be a poor approximation to reality occur when the distribution of air void radii is skewed (Pigeon). When there are a disproportionate number of air voids with small or large radii, the mean radius that the Powers spacing factor calculation is based on does not accurately represent the air void structure in the cement paste. The Philleo factor was developed specifically to overcome this limitation. To calculate the air void spacing, the Philleo factor assumes the same cubic lattice structure that the Powers factor assumes. The Philleo factor is different in that it allows the distribution of sphere radii to affect the calculation. This effect can be visualized by allowing different sized spheres to occupy the cubic lattice sites in Figure 4. When these different sphere sizes are representative of the sphere size distribution in the cement paste, an accurate representation of the air void structure is achieved. This is what Philleo accomplished in deriving his spacing factor.

The Powers spacing factor has been well established through the ASTM C457 test as the standard for predicting the frost resistance of concrete. There are proponents in favor

of using the Philleo factor in conjunction with this test, but many experimentalists point out that the two factors are very similar for most concretes. It appears that the debate will continue, but the Powers spacing factor will be used as the standard for the near future.

1.2.4 Experimental Determination of Spacing Factors

The current testing techniques used for determining both the Powers spacing factor and the Philleo factor are based on stereology. Two basic principles, which are convincingly proven by Hilliard, are used in these tests. The first principle is that the area fraction of a constituent in a slice through a volume is identical to the volume fraction of the same constituent within the volume, (given appropriate sampling volumes and areas). Similarly, the second principle is that the fraction of a constituent traversed linearly is proportional to the volume fraction of the same constituent within the volume. Again the linear traverse case requires appropriate samples of the volume.

These two principles can be used to great advantage in applied microscopy. In this case, they can be used to determine a three dimensional spacing factor from two dimensional data. The ASTM C457 test (ASTM '90) obtains the two dimensional data in the following way. First, a concrete specimen of adequate size is cut to expose a plane section of the interior microstructure. The specimen is then polished, allowing the surface to be viewed using a microscope. With the level specimen traversing linearly beneath the microscope at an appropriate magnification, constituents are measured out as the linear path intersects them. To obtain statistically significant results, the traversed path must usually be quite long. Since a technician is generally observing the specimen and measuring the features under the microscope, this person must spend a significant amount of time making these long and tedious measurements. The time required to analyze a single specimen can sometimes exceed four hours, leading to operator fatigue and possibly inaccurate data.

If an automated procedure could replace the current manual test, it would have the potential to improve the test in two significant ways. First, an automated procedure should improve the precision of the measurement significantly because an algorithm will analyze the same material consistently, eliminating possible human errors. Second, if the new procedure was implemented properly, it could significantly reduce the time required to perform the test. Image analysis techniques provide a means to achieve this type of automation.

1.3.1 Thesis Objective

There are two major problems that are inherent in the current ASTM C457 test for freeze-thaw durability which can be addressed by an automated procedure. These problems are poor statistical precision and extremely slow evaluation time. The lack of statistical precision in the current manual test comes from human error on the part of the technician performing the test. The slow evaluation time results from a manual procedure, which requires laborious effort. A procedure is developed in this thesis which has the potential to reduce both of these problems significantly. The procedure uses image analysis techniques to collect and process data, thereby automating these procedures.

The basic goal of this work is therefore:

To create and validate an image analysis system that measures accepted air void parameters that predict concrete performance.

Chapter 2 - Experimental Study

2.1 - Testing Issues

2.1.1 - Testing Development

To develop an effective new means of obtaining concrete air void parameters, the new method must be compared to a standard. The ASTM C457 test is the standard procedure currently used to determine air void parameters of concrete and will therefore be used in this study as a standard for comparison. The general principles of the ASTM C457 test will be adhered to by the new test, but the data will be collected and processed by original means which have not been used before. A brief review of the current ASTM C457 test is presented in the following section to make the comparison between the current procedure and the newly developed procedure clear.

2.1.2 - The ASTM C457 Test

Two basic procedures are outlined in the ASTM C457 test to determine air void parameters of concrete. The first procedure is called the linear traverse method, while the second is called the point count method. The point count method is not practical for adapting to an image analysis procedure, so this discussion will be limited to the linear traverse method. As briefly discussed in section 1.2.4, the linear traverse method involves the examination of a cut and polished section of concrete which exposes the interior structure of the material. The polished specimen is placed under a microscope and is moved along a linear path while it is being observed by a technician. The technician measures the linear distances traversed through each material constituent as the specimen moves. Because the specimen is finite in size, it is stopped when the edge of the material is reached. The specimen is then moved a small increment in a direction perpendicular to the original traverse and another linear traverse is begun. In this way, a significant linear distance can be examined on a relatively small sample.

From these measurements of linear chords through each material constituent, many of the physical parameters associated with the concrete microstructure can be calculated. These parameters and the equations used to calculate them are outlined next.

First, the total distances traversed through air voids and paste must be determined. These are denoted by "T_a" and "T_p" respectively, while the total distance traversed through paste and air voids is denoted by "T_t". "N" denotes the total number of air voids intersected during the linear traverse. The average chord length intersected by each air void is given by "l_{mean}", and the specific surface is represented by the symbol "α". As explicitly shown in equation form below, the specific surface is solely a function of "l_{mean}".

From the parameters defined above, the following information can be calculated.

Air content (A), in %:

$$A = \frac{T_a \ 100}{T_t} \tag{2.1}$$

Average chord length (l_{mean}):

$$l_{mean} = \frac{T_a}{N} \tag{2.2}$$

Specific surface (α):

$$\alpha = \frac{4}{l_{mean}} \tag{2.3}$$

Paste content p, in %

$$p = \frac{T_p * 100}{T_t} \tag{2.4}$$

Paste-Air ratio (p/A):

$$\frac{p}{A} = \frac{T_p}{T_a} \tag{2.5}$$

Powers spacing factor (L_{mean}):

For p/A<=4.342

$$L_{mean} = \frac{T_p}{4N} \qquad (2.6)$$

For p/A>4.342

$$L_{mean} = \frac{3}{\alpha}(1.4(1 + \frac{p}{A})^{1/3} - 1) \qquad (2.7)$$

It is important to keep in mind that all of the parameters determined in equations 2.1 through 2.7 above are determined statistically (Walker). Therefore the sample size covered by the linear traverse is significant. Recommendations for the traverse length in the ASTM C457 test relate to the average size of aggregates in the concrete. The traverse length is longer for large average aggregate sizes because the paste and voids affect the air void parameters, while aggregates are excluded from these calculations. Regardless of the specimen type, a significant length must be examined to gain statistical significance, which requires a great deal of time for a technician in front of a microscope. This issue will be explored further in the discussion of the new image analysis method.

2.1.3 - Specimens

Two concrete specimens were made at the Virginia Transportation Research Council (Lozev) using significantly different amounts of air entrainment chemicals. Both specimens were cut to expose a sixteen square inch surface and were then polished for a standard ASTM C457 test. The standard test was performed by a technician for both specimens and the results showed that their spacing factors were an order of magnitude different from one another, as shown in Appendix A. Other air void parameters were also observed to be markedly different for these two specimens. The specimens themselves were made using a type I/II cement, crushed granite, salicious sand, and a proprietary air entraining admixture from W.R. Grace.

In preparation for the new test method the specimens were polished further, using a final diamond grit size of one micron. To speed up the polishing process, both of the original specimens were cut into twenty smaller specimens before polishing began. Twelve specimens could be accommodated by the automatic polisher for a polishing run.

Therefore, twelve small specimens cut from each of the two original specimens were used in testing for this study, as shown in Appendix D. Numbering in the diagrams of Appendix D indicates the test number each specimen was used for. With the cutting and polishing completed, the specimens were ready for use in the new test method being developed for this study. It should be noted that the time required to obtain an adequate polishing finish varied from one specimen to another. This was generally attributed to the aggregate content of the individual specimen. Those specimens that contained more large aggregate material generally required more polishing time.

2.1.4 - Scope of the New Test Method

The time consuming nature of performing the current ASTM C457 test manually makes a more automated procedure very attractive (Oren). The test developed for this study uses a sample preparation technique along with a high contrast microscopy method to automate the classification of the material constituents under observation. Digital images obtained using this microscopy technique and a CCD camera can then be processed by a computer program which has been written for this project. The computer program linearly traverses the images and makes corrections for edge effects that result from cut off features on the boundaries of the images. The program then processes the linear traverse data and calculates air void parameters from it.

2.2 - Microscopy Background

2.2.1 - Differential Interference Microscopy

Differential interference contrast microscopy, (DIC), is a technique that offers excellent contrast when the material under observation displays physical relief. This technique can also exhibit high contrast when different media are being observed under the microscope. For reflected light applications of DIC microscopy, the basic geometry

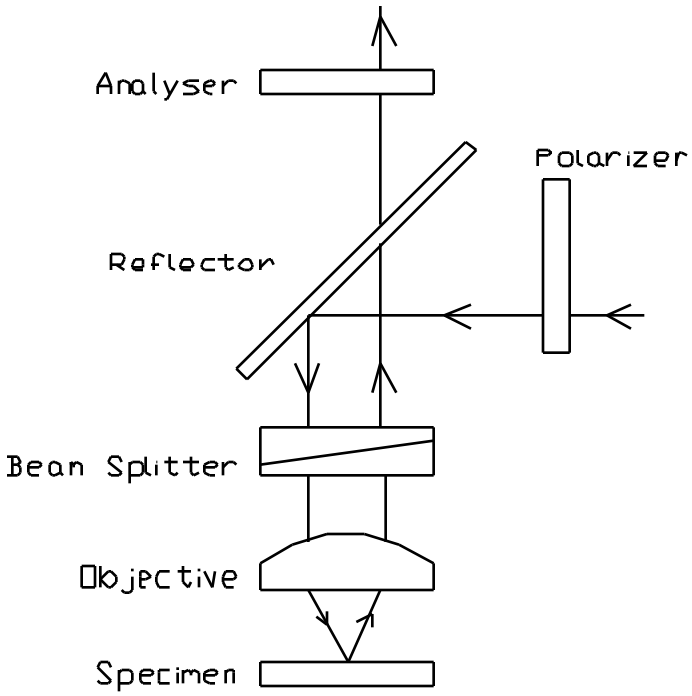

Figure 5. Optics for differential interference microscopy.

of the optics is presented in Figure 5. The method relies on differences in optical path distance, (OPD), between beams of light generated in the beam-splitter (Robinson). As shown in Figure 5, the incident light on the specimen first passes through a polarizer, strikes a reflector, and enters the beam splitter. The beam splitter divides the incoming light beam into two components which are slightly offset from one another. Both beams are focused onto the specimen by an objective lens and subsequently strike the specimen in adjacent locations. The two light beams return through the objective lens and are recombined as they travel through the beam splitter. If the specimen exhibits differences in height between the locations where the split beams strike the surface, the two beams will interfere with one another when they are recombined (DeHoff). This interference phenomenon causes extremely dark or light regions to appear in areas where the specimen height is above or below the focal plane. If the two beams are reflected by different media, a phase change difference can be imparted by the materials. The resulting interference from this phase change can also produce regions that are extremely dark or light.

A combination of the interference phenomena described above occur when properly prepared concrete is observed using DIC microscopy. If the specimen is polished properly, the physical relief in the specimen becomes very clear. Features such as air voids and cracks in the specimen appear very dark. This is due to a combination of two effects taking

place simultaneously. First, interference between light beams due to the physical relief inherent in these voids and cracks makes them appear dark. Second, the surfaces in the voids and cracks are not polished, making them poor light reflectors. This makes the voids and cracks in the concrete appear even darker than light interference alone would make them.

Contrast between aggregate materials and the cement paste in the concrete is also generated by the interference phenomena produced in DIC microscopy. The primary cause of the contrast generated here is once again height differences. The cement paste in concrete is a tangle of a wide variety of crystalline shapes when it is viewed under high magnification. At the magnification levels used to determine concrete air void parameters, this tangle of crystals appears as slight variations in height. Under a DIC microscope this means that some interference will take place. This interference in the paste produces a light gray region, since there are some cement paste crystals in the focal plane that reflect well, while other crystals outside the focal plane produce interference. Aggregate materials are much more homogeneous under high magnification than the cement paste that binds them together. Therefore, polished aggregate materials provide a highly reflective surface that results in very little interference under a DIC microscope. The result of this low interference is that aggregates appear close to white in color.

All of the contrast effects observed in concrete under a DIC microscope are significantly enhanced by proper polishing. The most effective level of polishing for this technique is significantly higher than is normally required for a standard ASTM C457 test. The extra polishing for this study was performed using an automated polisher, and therefore required a limited amount of labor.

2.3 - Image Collection

2.3.1 - Obtaining digital images

In order to use an image analysis technique to perform an ASTM C457 test, there must be a means of obtaining the digital image data. For this study, a black and white CCD camera with a C-mount was attached to the standard camera mount on a science grade Leica microscope operating in a reflected light mode. Differential interference contrast optics were designed into the microscope itself. The analyzer in these DIC optics was always set in the forty five degree position relative to the polarizer when images were captured. A frame grabber on a 486 computer allowed images to be obtained through Bioquant software. These digital images measured 512 pixels in width, 400 pixels in height and had

255 brightness values available in each pixel position. Each image occupied approximately one quarter of a megabyte, which allowed them to be stored on standard 1.44 megabyte diskettes. The images on disk were then taken to a Sun Sparcstation 10 and converted to a raw file format, which could be read by the image analysis program. This program is discussed further in the following section, and described in detail in Chapter 3.

2.4 - Image Analysis Program

2.4.1 - Image analysis program function

The purpose of the image analysis program in this new test method is to determine the air void parameters of the concrete from the data in raw digital image files. The program, presented in Appendix C, accomplishes this task in a few basic steps. A simplified description of these steps is provided in this section, while detailed information is deferred to Chapter 3. A decision was made to use the C programming language because of its coding efficiency and availability in the electrical engineering workstation laboratory at Virginia Tech, where the code was run.

The program first calculates a 128 by 128 element matrix which will be used later for edge correction calculations. These calculations are required because features in the images will often be partially cut off by the image boundary, which artificially alters their geometry. A series of images was made for each concrete sample that was analyzed, and therefore a number of tasks performed by the program are repeated for each image. The first of these repeated steps is to read the data from the image file into a two dimensional array. This is accomplished by assigning each pixel intensity value to an array location that corresponds directly to its position in the image. Once the image data is loaded into an array, it is available to the program for analysis.

The first portion of this analysis uses an operation referred to as thresholding (Ramesh). This thresholding operation is the procedure that is used to distinguish aggregate, cement paste and air voids from one another. In the raw images of the concrete the air voids appear dark, having low pixel intensity values. The cement paste appears gray, corresponding to intermediate intensity values, and the aggregates appear essentially white, corresponding to high intensity values. An example histogram taken

from one of the raw images used by the program illustrates this in Figure 6. Pixel intensity values below eighty four on the histogram correspond to air voids, while intensity values above one hundred seventy correspond to aggregate materials. Intensity values that lie between these two numbers correspond to cement paste. The program creates a new image using

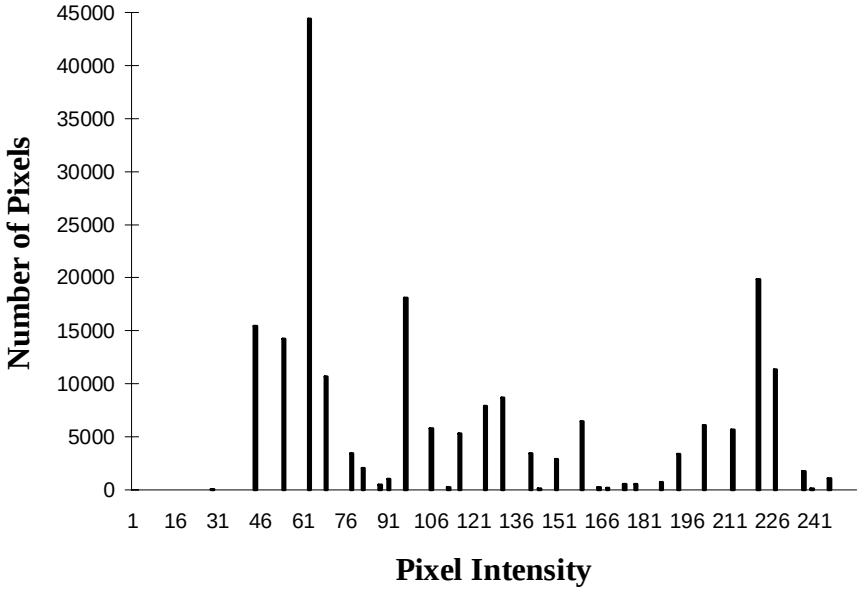

Figure 6. Example histogram from a sample image, (vod1).

this information, assigning the same value to each pixel that corresponds to air voids, another value to each pixel corresponding to paste, and a third value to each aggregate pixel.

Next, the program linearly traverses the labeled concrete image and stores the chord lengths of paste, aggregate and voids that it intercepts. Linear traverses are performed on each of the rows in the image and the process is repeated for all of the images in the series. The chord lengths for cement paste and air voids are stored in classes which are used in edge correction calculations that are detailed in Chapter 3. Air void parameters, including the Powers spacing factor, are calculated based on the accumulated linear traverse data from all of the images in the series. Edge correction calculations are

performed for the data and void parameters are calculated again based on this corrected information.

2.5 - Experimental Results

2.5.1 - Images

For each of the two samples made and previously analyzed using the ASTM C457 manual test, three sets of images were made to be analyzed using the program described in section 2.4.1. Six data sets were therefore created, each comprised of twenty images. The statistical significance of this sample size was determined during the analysis of each data set. Example images from two of these data sets are presented in Figures 7a and 7b. As previously noted in section 2.4.1, the aggregate, cement paste and void regions have unique ranges of gray scale values with only a few exceptions. These exceptions, such as cracking in aggregate regions, are dealt with by the image analysis program. The images in Figures 7a and 7b along with one hundred eighteen others, provided all of the raw data which was used to calculate void parameters for both specimens.

2.5.2 - Image analysis

The image analysis program, described in section 2.4.1 and chapter 3, was used to process data from six sets of images. Three of these image sets were collected from specimen c1v1, while the other three sets were collected from specimen c3v3. Test runs that used these collected images were numbered sequentially. Test two of specimen c1v1, for instance, used images collected from the four cut regions designated by a "2" in Appendix D. Five images were collected from random locations in each of the four cut regions designated by a "2" to make a total of twenty for test 2 of specimen c1v1. The same procedure was followed for each of the sequentially numbered tests performed on both specimens.

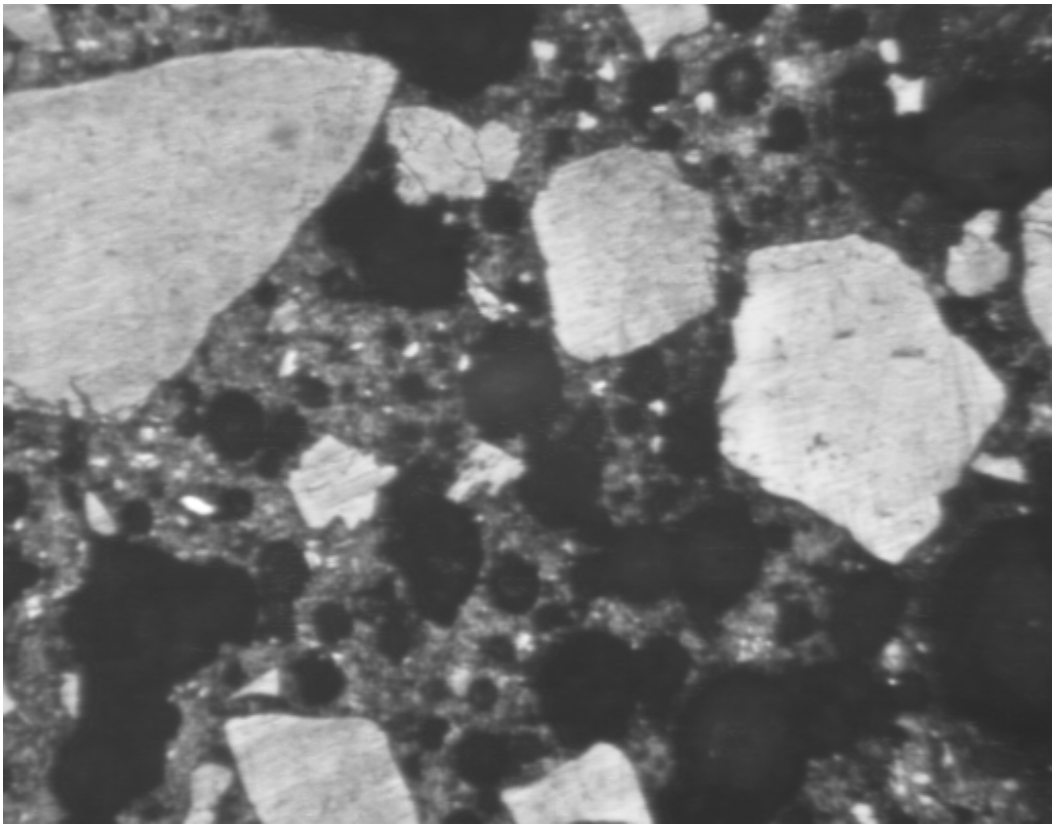

Figure 7a. DIC micrograph of specimen c3v3, (magnification 50X, image width 1.4 mm).

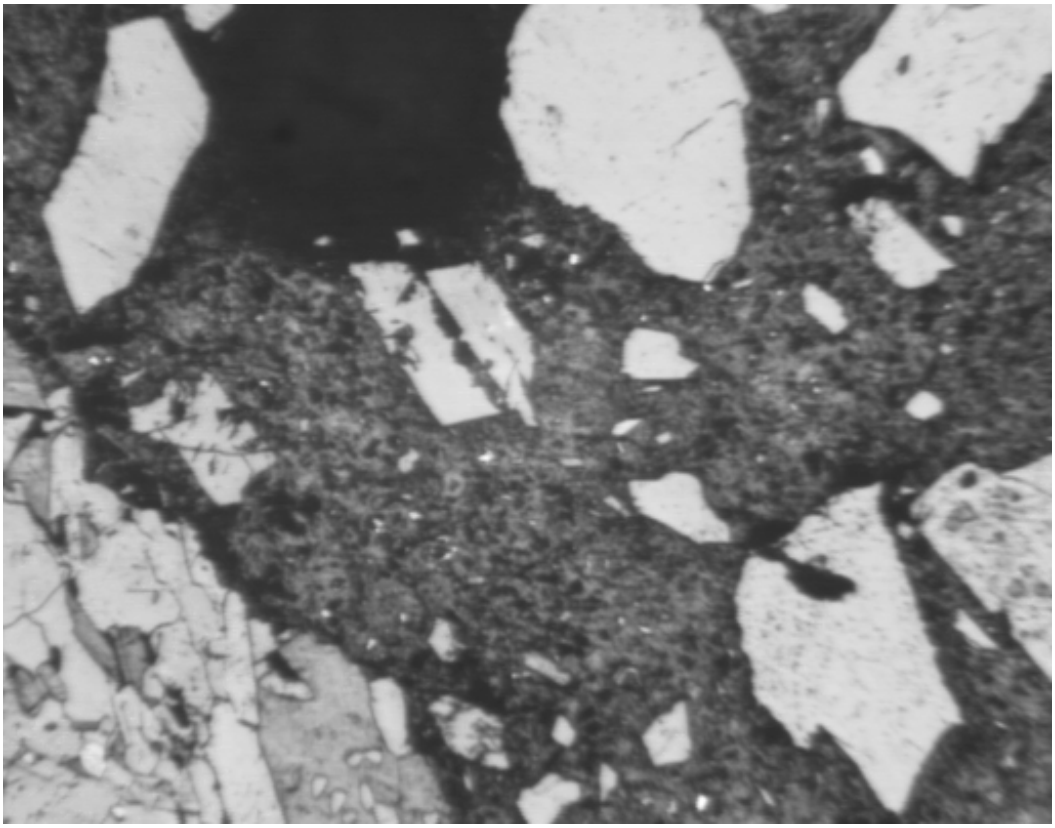

Figure 7b. DIC micrograph of sample c1v1, (magnification 50X, image width 1.4 mm).

The Powers spacing factor was calculated for each of the six data sets for comparison to the ASTM C457 results obtained by the Virginia Transportation Research Council, (VTRC). Figure 8 presents a comparison between the Powers spacing factor obtained by VTRC and the three image data sets analyzed for specimen c1v1 before edge correction. The dark gray bar, test one, is the VTRC value while tests two through four are values calculated using the image analysis program. Error bars extend one standard deviation from the mean value. The standard deviation for the VTRC test represents the standard deviation expected by ASTM for tests that are performed in different labs. The standard deviations on each Powers spacing factor were obtained from the statistical distributions of chord lengths intercepted in each test. Clearly, the values calculated using the image analysis method are significantly lower than the expected value provided by VTRC. However, these values have not been corrected for edge effects. The image analysis results corrected for edge effects for sample c1v1 are presented in Figure 9.

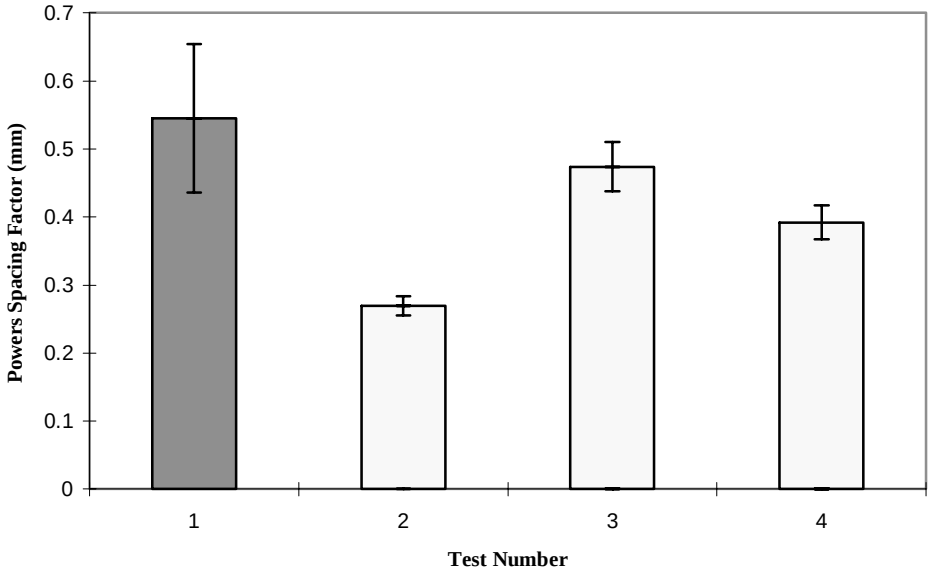

Figure 8. Measured Powers spacing factors for sample c1v1.

This correction brings the values significantly closer to the VTRC value. Tests three and four are within one standard deviation of the VTRC reference value while test two differs significantly from the VTRC value in the edge corrected graph.

The likeliest explanation for the discrepancy seen in test two is that local distributions of void sizes were larger in the areas sampled for test two, decreasing the spacing factor. This is confirmed by looking at the mean chord intercept encountered during test two. It is larger than the mean chord intercepts in tests three and four, as observed in Appendix B. The standard deviations for all three image analysis tests on sample c1v1 are quite small, confirming that local effects in the sample are the likely cause of any discrepancy.

A brief comparison of the areas and lengths traversed by the VTRC test and the image analysis test will provide significant insights in comparing the two tests. For the VTRC test of sample c1v1, a length of 228.6 cm was traversed, but these traverses were spread out over a 68 square centimeter area. The total length traversed over the twenty

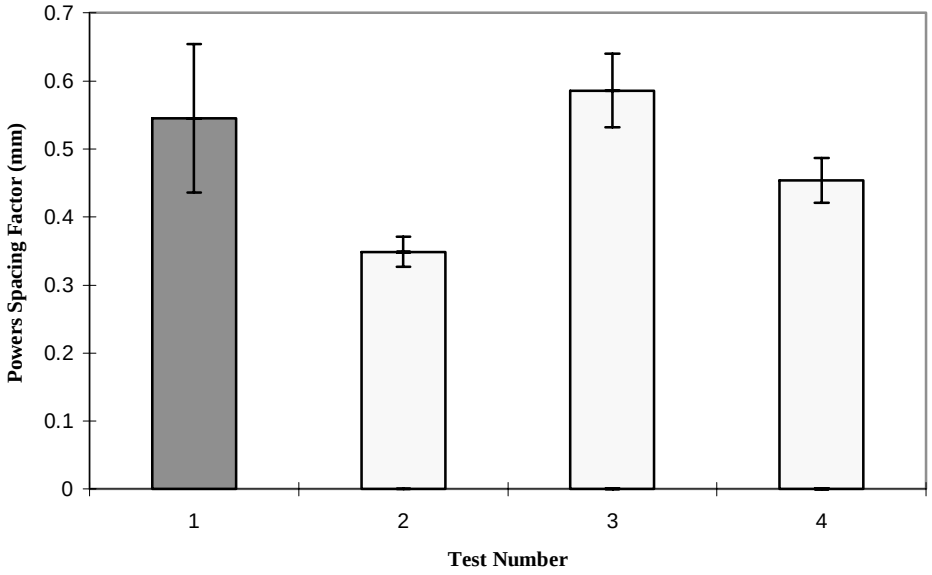

Figure 9. Measured Powers spacing factors
corrected for edge effects, (sample c1v1).

images analyzed for each image analysis test is 1120 cm. These traverses are performed over an area of 0.31 square centimeters. The length traversed in the image analysis test is more than adequate to meet the requirements of the ASTM C457 test. However, discrepancies between the image analysis calculations and the standard ASTM test can result from differences between air void characteristics in the local areas sampled. The three image analysis tests on specimen c1v1 demonstrate that these local effects are present, but can be quantified. The standard deviation of the three spacing factors calculated by image analysis for specimen c1v1 is 0.12 millimeters. This value is comparable to the standard errors experienced by performing ASTM C457 tests in different laboratories.

The Powers spacing factors calculated for specimen c3v3 are presented in Figures 10 and 11. Again, the significant effect of edge correction calculations are observed here. For the edge corrected data, all three image analysis spacing factors are within one standard deviation of the VTRC reference value. Local variations in the air void structure

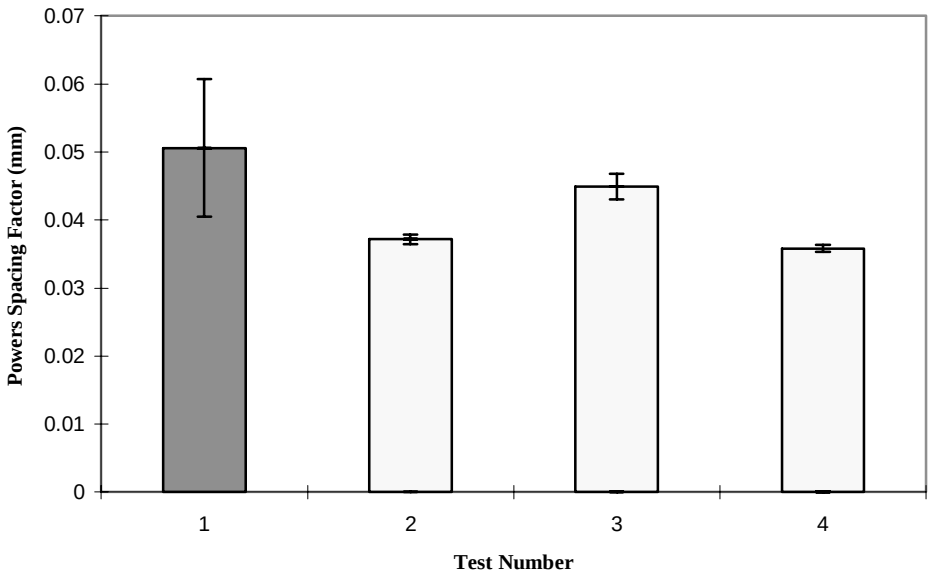

Figure 10. Measured Powers spacing factors for sample c3v3.

are observable in the variations between these three calculations, but none of them are statistically significant, (greater than one standard deviation).

Another significant interpretation of the data presented in Figures 8 through 11 is a comparison between the Powers spacing factors calculated for each specimen. The spacing factor for specimen c1v1, as calculated by VTRC, is an order of magnitude greater than the spacing factor calculated for specimen c3v3 by VTRC. This order of magnitude difference in spacing factors is duplicated by the image analysis results when the data is viewed qualitatively. This is significant because predictions of concrete freeze-thaw durability are often based on the value of the Powers spacing factor. It is generally accepted that a value of 0.2 mm or less for the spacing factor is associated with a freeze-thaw durable concrete. Under this criterion, sample c3v3 would be labeled as freeze-thaw durable based on the image analysis test, while sample c1v1 would not. This would be an accurate assessment based on the results provided by VTRC.

Taken as a whole, the calculations performed here have shown that statistically significant values for concrete air void parameters can indeed be obtained using image

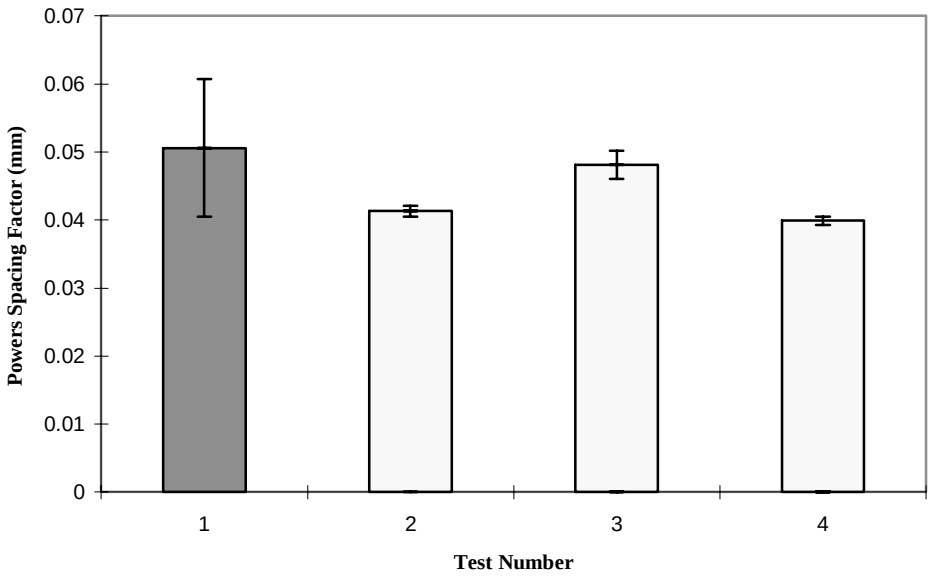

Figure 11. Measured Powers spacing factors corrected for edge effects, (sample c3v3).

analysis. A great deal of further study would be required to allow the techniques used here to become part of a standard, but the potential has now been shown.

Chapter 3 -The Image Analysis Program

3.1 - How the Program Works

3.1.1 - Implementation of the Image Analysis Program

The general functions performed by the image analysis program written for this study have been summarized in section 2.4.1. This chapter describes the details of the logic and theory used to write the program itself, which is presented in Appendix C. The program is fully documented to aid the user in the interpretation of the code. This discussion will proceed in the order of the functions performed by the program.

First the program loads header files, defines variables and functions, and then initializes variables. Next, threshold values are stored in the variable "thr" for later use in a function subprogram. These "thr" values are determined for each collected raw image by interactively thresholding (Russ) the image in the Bioquant PC software as the digital images are being captured. This software allows the user to view any threshold instantly by selecting a desired intensity on a slider bar. When the proper threshold is selected, all areas corresponding to a specified concrete constituent will be highlighted. A function subprogram is subsequently called which produces a matrix for edge effect calculations. These calculations have been developed in the microscopy literature and have been used for many applications (Cruz-Orive). The following derivation and discussion, which is adapted from the work done by Dewey et. al., provides the necessary background for understanding these calculations.

3.1.2 - Correction for edge effects

For a lineal analysis, such as the linear traverse test used in ASTM C457, a field of view is scanned along one or more distinct test lines of length "L". Features traversed by these test lines will be intercepted by the line over a chord length "l". The midpoint of the

chord is used for a reference point, and intercepts of length "l±dl/2" are grouped in individual size classes. When a chord passes through a feature that is only partially included in the field of view, the feature is truncated by the frame edge (Attiogbe). For every chord length "l" that is less than or equal in magnitude to "L", the following method will be applicable.

"f(l)" will be assumed to be the continuous function that represents the relative frequency distribution of chord lengths, which can also be thought of as the probability density of chord lengths. "$f(l_i)dl$" will then be the probability that a chord has a length of "$l_i \pm dl/2$", where dl has infinitesimal length. "l" can have values such that it lies between 0 and "l_{max}" where "l_{max}" has a value that is smaller that the frame length, "L".

If N_L is then the true number of chords intercepted per unit length, then the finite approximation to the true number of chords per unit length is given by equation 3.1.

$$N_L(i) = N_L f(l_i)dl \qquad (3.1)$$

Chords with a length of "$l_i \pm dl/2$" are grouped together in a class. The number of chords in the class is made up of two parts, n_1 and n_2. n_1 represents the number of chords with length "$l_i \pm dl/2$" which have not been cut off by the frame edge, while n_2 is the number of chords that have been artificially shortened because they are cut off by the frame edge. These cut off features have a measured length of "$l_i \pm dl/2$".

If the center of a chord with length "l_i" is located within the field of view and not more than "$l_i/2$" outside the field of view, it will be visible. The product of the true number of "l_i" chords per unit length and the distance along which an "l_i" chord center can be located produces the total number of measured chords resulting from chords with a true length of "l_i". The total number of measured chords is therefore given by equation 3.2.

$$n(i) = N_L(i)(L+l_i) \qquad (3.2)$$

A chord with a length "l_i" that is visible in the field of view will not be intersected by an edge when its midpoint is not located closer than "$l_i/2$" to an edge. The probability that a visible chord length "l_i" will not be intersected by an edge is given by a ratio. The ratio, presented as equation 3.3, has the length within the field of view along which the midpoint of an "l_i" chord can be located and not cut off in the numerator. The denominator is given by the total length in which an "l_i" chord can be located and still be at least partially visible within the field of view.

$$P(l_{ia} \mid l_i) = \frac{L - l_i}{L + l_i} \qquad (3.3)$$

The expected number of chords visible in the field of view with length "l_i" and not intersected by a frame edge is therefore the product of the total number of visible "l_i" chords and the probability that the visible chord will not be cut off.

$$n_1 = n(i)P(l_{ia} \mid l_i) \qquad (3.4)$$

In order to determine the number of chords which have been cut off by a frame edge, chords of length "l_j" must be examined which have a length greater than or equal to "l_i". A chord of length "l_j" will be visible in the image field of view if the chord midpoint is located within the viewing field or not greater than "$l_j/2$" outside of the viewing field. The total number of chords in the field of view with length "l_j" is given by equation 3.5.

$$n(j) = N_L(j)(L+l_j) \qquad (3.5)$$

The probability that a chord of length "l_j" will be cut off by a frame edge is given by a ratio. The numerator of this ratio contains the length along which the midpoint of an "l_j" chord can be positioned which causes the chord to be cut off. The denominator contains the length along which the midpoint of an "l_j" chord can be positioned which causes the chord to be at least partly visible in the image field of view.

$$P_{cut}(l_j) = \frac{2l_j}{L + l_j} \qquad (3.6)$$

The probability that a chord length of "l_j" will contribute to any smaller class sizes than itself is equal for each of these smaller classes. The probability of "l_j" being a truncated chord length is therefore "dl/l_j". The expected number of visible chords of length "l_j" that are cut off by a frame edge and result in a chord of length "$l_i \pm dl/2$" is therefore given by equation 3.7.

$$n_2(j) = n(j)P_{cut}(l_j)dl/l_j \qquad (3.7)$$

The total number of chords that appear to have length "l_i" because they are cut off can be obtained by substituting equation 3.6 into equation 3.7 and integrating, which results in equation 3.8.

$$n_2 = 2\left(\int_{l_i}^{l_{max}} N_L f(l_j)\,dl\right)dl \qquad (3.8)$$

Summing n_1 and n_2 from equations 3.4 and 3.8 gives the total number of chords of apparent length "$l_i \pm dl/2$" in the field of view.

$$n(i)^* = n_1 + n_2 \qquad (3.9)$$

The number of chords of apparent length "$l_i \pm dl/2$" per unit length is obtained by dividing both sides of equation 3.9 by "L", which is the frame length.

$$N_L(i)^* = \frac{n(i)^*}{L} \qquad (3.10)$$

For class sizes of finite width and "f(l)" assumed to be uniformly distributed within each class, equation 3.10 can be integrated over a class "i" to get the number of chords per unit length with an apparent length within the class "i". Equation 3.10 can be alternatively expressed as a sum, which leads to a relationship between apparent and actual numbers of chords per unit length. This relationship can be expressed in matrix form as equation 3.11. Here the dimensionless coefficients, K_{ij}, form an upper triangular

$$\{N_L(i)^*\} = [K_{ij}]\{N_L(i)\} \qquad (3.11)$$

matrix. The elements of this K_{ij} matrix are presented in equation 3.12, where "Δl_i" is the class size.

(3.12)

$$K_{ij} = \begin{cases} \dfrac{L - dl_i + \Delta l_i}{L} & (i = 1...s;\ j = i) \\ \dfrac{2\Delta l_i}{L} & (i = 1...s-1;\ j = i+1...s) \\ 0 & (i = 2...s;\ j = 1...i-1) \end{cases}$$

By inverting the matrix K_{ij}, the actual number of chords per unit length can be computed by equation 3.13.

$$\{N_L(i)\} = [\alpha_{ij}]\{N_L(j)^*\} \qquad (3.13)$$

where α_{ij} is the inverse of K_{ij}. To compute the α_{ij} matrix for the images used in this study, a K_{ij} matrix was computed using the following values.

$$L = 1.4000 \text{ mm}$$
$$\Delta l = 0.0109 \text{ mm}$$

This K_{ij} matrix was a square upper triangular matrix with 128X128 elements. The matrix was inverted using Mathematica, resulting in the upper triangular matrix α_{ij}. Because the matrix was so large, it was not possible to enter its values directly into the image analysis program. Instead, it was determined that a linear fit to the elements of each row, (excluding the diagonal elements), produced an accurate representation of α_{ij}. The diagonal elements, which were not consistent with these curve fits, were entered separately. Equation 3.11 could then be used to obtain edge corrected chord lengths from class data.

3.1.3 - Image labeling

Before void parameters can be determined from raw image files, the images must be labeled. The subroutine "threshim" accomplishes this by assigning a number to each pixel in the image that corresponds to a particular concrete constituent. These new pixel values are stored in the original image array. A second procedure called "framing" is then performed by the "frm" subprogram. This subprogram assigns each of the pixels on the outside border of the image the same value assigned to aggregates. The reason this frame is used in the image will be discussed in section 3.1.4. All of the labeling functions described here are performed on each of the images in a data set.

3.1.4 - Calculating void parameters

With an image labeled accurately for the locations of air voids, aggregate and cement paste, image analysis to obtain air void parameters can be undertaken. In the same way that the manual ASTM C457 test uses a linear traverse procedure, the image analysis program will also perform a linear traverse. Each row in an individual image, which has a length of

1.4 mm under 50X magnification, is scanned by the program. The chord lengths of any air voids or paste regions that are encountered are recorded and saved in classes, according to their length. 128 size classes are available to store these chord lengths, which will be used for edge effect calculations and in computing air void parameters. When these air void chord lengths are placed in size classes, a distinction is not made between entrained air voids and entrapped air voids. Chord lengths associated with entrapped air voids are not normally counted in a standard ASTM C457 test (Pleau). However, the samples used in this test contained very few entrapped air voids, so this did not significantly affect the measurements that were made.

Cracks and other flaws in aggregates, which may appear to be air voids when threshold labeling is done, are sorted out of the calculations. This is accomplished when the program checks the material constituent on the ends of each chord length collected. If aggregate is located on both ends of the chord, the chord is considered aggregate.

The trigger used to begin recording a chord length in the program is a change in material constituent encountered during a linear traverse. If a feature is on an edge, this could prevent the feature from being counted. To solve this problem, all of the edge pixels in each image were labeled as aggregates using the framing subprogram. Because the aggregate material constituent is not used in calculating air void parameters, it did not have an effect of them. However, these image pixels allow features at or near the edge to be detected, since they will be recognized as different from aggregate.

Once all of the chords in a set of images have been collected and placed in classes, the length of air voids traversed and the length of cement paste traversed are calculated. With this information and the chord lengths known, the equations from section 2.1.2 are used by the "powrs" subprogram to compute air void parameters, including the Powers spacing factor. The standard deviation of the Powers spacing factor is also computed based on statistical analysis of the collected chords (Snyder). All of the results from these calculations are presented in Appendix B for the images analyzed in this study.

Edge correction calculations are performed in the program by multiplying the edge correction matrix derived in section 2.1.2 by the vector composed of 128 chord length classes. The product of this multiplication is the vector of chord lengths corrected for edge effects. With this vector of chord lengths, the void parameters including the Powers spacing factor are calculated again by the "powrs" subprogram. With these calculations completed, the program writes the results to the screen and ends.

Chapter 4 - Conclusion and Future Work

4.1.1 - Conclusion

The ASTM C457 test of concrete materials, which is used to calculate air void parameters including the Powers spacing factor, has been shown by Powers and others to provide significant insights into concrete performance. In particular, the freeze-thaw durability of concrete has been related to values of the Powers spacing factor less than approximately 0.2 mm in many studies, (Mehta). These studies indicate that for a spacing factor of less than 0.2 mm, concrete has a significantly better freeze-thaw durability than those with spacing factors above this threshold. Two samples analyzed by the Virginia Transportation Research Council using a manual ASTM C457 test were used in this study to demonstrate a new test method for determining the Powers spacing factor, (among other air void parameters).

The new test method involved preparing highly polished sections of concrete and subsequently viewing them using a differential interference contrast microscopy method. Digital images captured using the microscope were processed by an image analysis program, which computed the air void parameters of the concrete material. Spacing factors were calculated using the image analysis method for each of the two specimens. The spacing factors for both specimens had been previously determined to be distinctly different according to VTRC results.

The image analysis calculations performed by the program written for this study showed that the results from the new test method compare quite well with the manual method recommended by ASTM. Five of the six tests carried out using the new test method were within one standard deviation of the manual test results obtained by VTRC. The measurements obtained using the new test also reflected the order of magnitude difference between the Powers spacing factors of the two specimens. One of the samples tested, c1v1, had a spacing factor greater than that recommended for freeze-thaw durable concrete while the other, c3v3, had a spacing factor less than this recommended value according to VTRC. The close correlation between the results for the new method and the

manual method are significant because it indicates that the new test method is capable of distinguishing between freeze-thaw durable concrete and concrete that cannot withstand freezing and thawing cycles. This conclusion can only be drawn on a limited basis, however, because the samples used in this test are not representative of all concrete materials. Extensive testing on many different types of concrete would be required to confirm the validity of the test for use with all concrete materials.

The polishing process required to perform the new test is the major drawback of the method. Although the polishing can be performed by automatic polishing equipment, it is time consuming. The variability of the polishing rate for the small specimens used is also troublesome, since they must be checked periodically during the polishing process to stop the polishing at the appropriate time. Even with these drawbacks, a significant time savings can be achieved using the new test method rather than the manual ASTM C457 test. With an automated stage, images can be collected in minutes and the image analysis program requires approximately two minutes to process twenty images. Several hours are required for polishing, but a technician must only be present near the end of the polishing process to check for proper finishing results.

Based on the results obtained in the tests performed for this study, an image analysis test method is a viable option for obtaining air void parameters of the concrete used in this study. The capability to distinguish between aggregate, cement paste, and air voids in the concrete samples used here was the key to making this possible. Significantly further study will be required to determine the new test's applicability to the wide variety of concrete materials currently in use.

4.2.1 - Future Work

Based on the promising results obtained using an image analysis method to obtain ASTM C457 air void parameters in this study, further research into the use of this type of test appears to be worthwhile. Researchers should be aware of the time drawbacks presented by the polishing procedure that is required for the test. However, once proper polishing has been attained, the methods used in the image analysis program in Appendix C produce statistically significant results. Other researchers have attempted to use image analysis to obtain air void parameters in the past, but their methods always had significant problems with identifying aggregate materials in the concrete. The results of this study

indicate that this problem has been overcome using the combination of a sample preparation technique, microscopy method and an image analysis program.

If the methodology used in conducting tests for this study can be shown to work for a wide variety of concrete materials, it should be considered for incorporation into the current ASTM C457 standard. This process would require a great deal of work, but could eventually result in a standard procedure that produces accurate results with less required technician labor.

References

ASTM, "Standard Test Method for Microscopical Determination of Parameters of the Air-Void System in Hardened Concrete," (ASTM C 457-90), *1990 Annual Book for ASTM Standards*, Vol. 4.02, American Society for Testing Materials, Philadelphia, Pa., 1990, pp. 232-244.

ASTM, "Standard Terminology Relating to Concrete and Concrete Aggregates," (ASTM C 125-93), *1993 Annual Book for ASTM Standards*, Vol. 4.02, American Society for Testing Materials, Philadelphia, Pa., 1993, pp. 59-61.

Attiogbe, E.K.; Darwin, D.; "Correction of Window Size Distortion of Crack Distributions on Plane Sections," *Journal of Microscopy,* Vol. 144, Pt. 1, October 1986, pp. 71-82.

Cruz-Orive, L.M., "Distribution-Free Estimation of Sphere Size Distributions From Slabs Showing Overprojection and Truncation, With a Review of Previous Articles," *Journal of Microscopy,* Vol. 131, Pt. 3, September 1983, pp. 265-290.

DeHoff, R.T.; Rhines, F.N.; *Quantitative Microscopy,* McGraw Hill Book Company, New York, 1968, pp.45-76.

Dewey, G.R., "Image Analysis of Air Voids in Air-Entrained Concrete," An unpublished report, Available from The University of Kansas Center for Research, Inc., Structural Engineering and Engineering Materials, SM Report No. 29, August 1991.

Gutmann, P.F., "Bubble Characteristics as They Pertain to Compressive Strength and Freeze-Thaw Durability," *Materials Research Society Symposium Proceedings*, Vol. 114, 1988, pp. 271-277.

Hilliard, J.E., "Measurement of Volume in a Volume," Chapter 3, *Quantitative Microscopy*, McGraw Hill Book Company, 1968, pp. 45-77.

Lozev, M.G.; Lane, D.S.; Clemena, G.G; Nakhleh, N.J.; "Initial Laboratory Studies of the Nondestructive Evaluation of Concrete Consolidation Using a Pulsed Ultrasonic Interferometer," Virginia Transportation Research Council - Final Report, February 1996.

Mehta, P.K.; Monteiro, P.J.M., Concrete - Structure, Properties, and Materials, Prentice Hall, Englewood Cliffs, New Jersey, 1993.

Oren, G.M.; Marks, V.J.; Dubberke, W.G.; "Image Analysis of Portland Cement Concrete and Asphalt Concrete Pavements Using Scanning Electron Microscope Images," *Transportation Research Record 1458,* pp. 20-25.

Philleo, R.E., "A method for Analyzing Void Distribution in Air Entrained Concrete," *Cement, Concrete and Aggregates,* CCAGDP, Vol. 5, No. 2, Winter 1983, pp. 128-130.

Pigeon, M.; Lachance, M.; "Critical Air Void Spacing Factors for Concretes Submitted to Slow Freeze-Thaw Cycles," *American Concrete Institute Journal.*

Pleau, R.; Plante, P.; Gagne, R.; Pigeon, M., "Practical Considerations Pertaining to the Microscopical Determination of Air Void Characteristics of Hardened Concrete

(ASTM C457 Standard)," *Cement, Concrete, and Aggregates,* CCAGDP, Vol. 12., No. 2, Summer 1990, pp. 3-11.

Powers, T.C., "Void Spacing as A Basis for Producing Air-Entrained Concrete," *Journal of the American Concrete Institute,* Vol. 25, 1954, pp. 741-760.

Ramesh, J.; Kasturi, R.; Schunck, B., Machine Vision, McGraw Hill, Inc., New York, 1995.

Robinson, P.C.; Bradbury, S., Qualitative Polarized Light Microscopy, Microscopy Handbooks - Royal Microscopical Society, Oxford Science Publications, 1992.

Russ, J.C., Computer-Assisted Microscopy - The Measurement and Analysis of Images, Plenum Press, Raleigh, North Carolina, 1990.

Snyder, K.; Hover, K.; Natesaiyer, K., "An Investigation of the Minimum Expected Uncertainty in the Linear Traverse Technique," *Cement, Concrete and Aggregates,* CCAGDP, Vol. 13, No. 1, Summer 1991, pp. 3-10.

Walker, H.N., "Formula for Calculating Spacing Factors for Entrained Air Voids," *Cement, Concrete, and Aggregates,* CCAGDP, Vol. 2, No. 2, Winter 1980, pp. 63-66.

Appendix A

Specimen and Test #	Total Specimen Travel (cm)	Mean Chord Intercept (mm)	Paste to Air Ratio	Specific Surface (1/mm)	Powers Spacing Factor (mm)
c1v1 - Test 1	228.6	0.3640	>4.342	11.0	0.5447
c3v3 - Test 1	239.4	0.0911	<4.342	43.9	0.0506

Void parameters obtained by the Virginia Transportation Research Council.

Appendix B

Specimen and Test #	Total Specimen Travel (cm)	Mean Chord Intercept (mm)	Paste to Air Ratio	Specific Surface (1/mm)	Powers Spacing Factor (mm)
c1v1 - Test 2	1120	0.2211	>4.342	18.1	0.3488
c1v1 - Test 3	1120	0.1837	>4.342	21.8	0.5855
c1v1 - Test 4	1120	0.1142	>4.342	35.0	0.4542
c3v3 -Test 2	1120	0.0834	<4.342	47.9	0.0414
c3v3 - Test 3	1120	0.0770	<4.342	51.96	0.0481
c3v3 - Test 4	1120	0.0862	<4.342	46.38	0.0399

Edge corrected void parmaters obtained using image analysis.

Specimen and Test #	Total Specimen Travel (cm)	Mean Chord Intercept (mm)	Paste to Air Ratio	Specific Surface (1/mm)	Powers Spacing Factor
c1v1 - Test 2	1120	0.1748	>4.342	22.9	0.2697
c1v1 - Test 3	1120	0.1517	>4.342	26.4	0.4738
c1v1 - Test 4	1120	0.1016	>4.342	39.4	0.3920
c3v3 - Test 2	1120	0.0784	<4.342	51.0	0.0371
c3v3 - Test 3	1120	0.0729	<4.342	54.9	0.0449
c3v3 - Test 4	1120	0.0808	<4.342	49.5	0.0358

Void parameters obtained using image analysis without edge correction

Appendix C

This appendix contains a proprietary algorithm which is not presented here. If you have an interest in gaining access to the code, please contact Dr. John C. Duke, Jr. at jcduke@vt.edu.

Appendix D

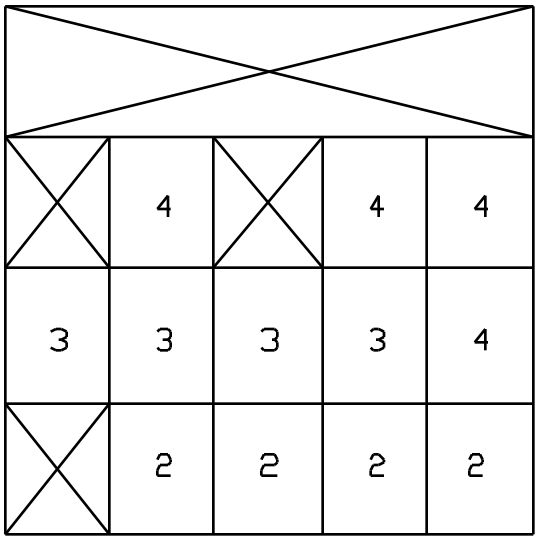

Sample C1V1, numbering corresponds to image analysis test number.

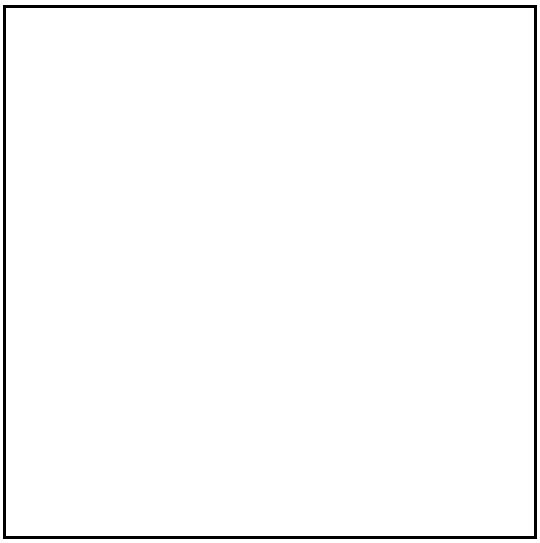

Sample C3V3, numbering corresponds to image analysis test number.

Vita

Michael Scott earned a bachelors degree in Mechanical Engineering from Texas A&M University where he held a Lechner scholarship for four years and graduated as a University Honors Fellow in 1995. Mr. Scott earned his Master of Science degree in Engineering Mechanics from Virginia Tech in 1997. He has worked as a graduate research assistant at Los Alamos National Laboratory and the Virginia Transportation Research Council on problems involving image analysis and materials evaluation. He currently holds an NSF Fellowship in the Center for Infrastructure Assessment and Management at Virginia Tech, where he continues his research in pursuit of a Ph.D. degree.